Multi-Camera and BIM-Based Benchmarking of Building Evacuation Parameters

Diran Yu[1], Abdul-Majeed Mahamadu[1], Weiwei Chen[1,2], Yang Su[1], Fujia Lyu[1], Jieyu Chen[3], Jiaxu Huang[3], Nan Li[3]

[1] The Bartlett School of Sustainable Construction, University College London (UCL), UK
[2] Division D: Civil Engineering, Engineering Department, University of Cambridge, UK
[3] Department of Construction Management, Tsinghua University, China
diran.yu.22@ucl.ac.uk, a.mahamadu@ucl.ac.uk, weiwei.chen@ucl.ac.uk, yang.su@ucl.ac.uk, fujia.lyu.24@ucl.ac.uk, chenjiey22@mails.tsinghua.edu.cn, hjx21@mails.tsinghua.edu.cn, nanli@tsinghua.edu.cn

Abstract –

As VR evacuation training and performance-based egress design increasingly rely on simulation, their credibility depends on empirical, space-specific motion benchmarks. However, VR evacuation research often lacks empirical, area-specific motion parameters for calibration. We demonstrate benchmark values from a full-scale multi-floor drill, reconstructed from multi-camera video as 2D trajectories in lobbies and corridors and 3D trajectories on stairs. An automated pipeline with YOLOv11 detection, DeepSORT tracking, and BIM-based calibration provides kinematics and crowd metrics, including speed, acceleration, local density, flow $q = \rho v$, and route choice. Corridors enabled the fastest travel with a mean of about 2.1 m/s. The lobby was slower at about 1.2 m/s with faster peripheral lanes. Stairs were slowest at about 0.52 m/s on landings and 0.39 m/s on flights. The fundamental diagram by local density ρ reveals three systems: free flow $\rho<3$ persons/m^2, collective flow $3\leqslant\rho\leqslant5$, and congested flow $\rho>5$. As ρ approaches 3 - 4, accelerations decay while mean speed remains stable. At $\rho\geqslant5$, speeds decline, and stop-and-go waves appear. Bottlenecks commonly formed at doors and stair portals, and exit usage was uneven. The Evacuation Parameter Benchmark Library derived here supports calibration of VR drills and agent-based models and informs performance-based egress design grounded in measured behaviour. The findings will be interpreted as building-specific empirical benchmarks derived from a moderate-scale drill, rather than universally transferable evacuation parameters.

Keywords –

Evacuation Simulation, Computer Vision, Pedestrian Dynamics, Trajectory Analysis, Building Safety, Data Benchmarking

1 Introduction and Background

1.1 Motivation and Scope

Immersive VR and agent-based evacuation simulation are increasingly used for training, design evaluation, and research because frequent full-scale multi-floor drills are costly, disruptive, and difficult to repeat under controlled conditions [1–3]. However, the credibility of VR-based findings depends strongly on calibration: the microscopic rules that govern walking, turning, merging, and vertical movement are sensitive to local geometry (width changes, corners, doors, landings), visibility, and interaction opportunities.

Reliable motion benchmarks that are space-specific are essential for calibrating walking, turning, and interaction in VR evacuation studies. Many implementations still apply a single speed cap or a uniform density–speed curve across heterogeneous spaces, which induces bias between lobbies, corridors, and stairwells [4–8]. Multi-camera tracking, person re-identification, and crowd-density estimation now enable reusable parameters to be extracted from real drills [4–8]. Nevertheless, consistent coordinates across cameras and floors, rigorous error control, and area-wise calibration are still underdeveloped, which limits transferability and credibility in VR and agent-based models [4,7]. The present study analyses multi-floor drill data, reconstructs 2D trajectories in lobbies and corridors and 3D trajectories on stairs, and provides multi-area benchmarks that can be used directly for model calibration.

1.2 Key Concepts and Terminology

A particle-to-collective view of pedestrian dynamics is adopted. Local density ρ in persons per square meter and mean speed v define the flow q through $q=\rho v$.

Operating regimes are partitioned by ρ to align with engineering practice. Free flow corresponds to $\rho<3$ with limited interactions. Collective flow corresponds to $3 \leqslant \rho \leqslant 5$ with coordination and speed regulation. Congested flow corresponds to $\rho>5$, where impediments and stop-and-go may occur [4,6–8]. Stair geometry motivates a stairway slowdown factor, typically yielding lower speeds on flights than on landings. Lobbies and corridors often exhibit edge preference with faster peripheral lanes along walls or railings [5,6,8]. The density–speed–acceleration relations later support the identification of acceleration decay zones and speed drop thresholds and serve as parameter inputs for VR scenes.

1.3 Related Work and Research Gap

Video-driven crowd research has progressed along three questions: who is present, where people move, and how many are there. Multi-camera detection and re-identification enable continuous trajectories across views and provide quantifiable kinematics for building evacuation [4,5,7]. Machine-vision density estimation delivers local crowding without markers and supports capacity evaluation and risk assessment [8]. Detector families continue to evolve, and the latest YOLOv11 offers improved accuracy–efficiency trade-offs for large-scale automated video processing [9–11]. Despite these advances, space-resolved distributions of speed and acceleration for lobbies, corridors, and stairwells remain insufficiently documented. A unified spatial frame that merges multi-camera trajectories, BIM coordinates, and density–speed–acceleration relations with transparent quality controls is still uncommon [4,7].

1.4 Positioning and Contributions

This work serves as a multi-area evacuation benchmarking resource for VR calibration and performance-based egress design. Four contributions are delivered. First, an automated pipeline integrates multi-camera video with BIM alignment and outputs reusable 2D and 3D trajectories with quality records [4,5,7]. Second, speed and acceleration profiles are reported for lobbies, corridors, and stairs with landings separated from flights, and a stairway slowdown together with an edge-preference index is quantified. Third, a density-based fundamental diagram is constructed. Acceleration decays markedly as ρ approaches 3–4 while mean speed remains stable. When ρ reaches 5 or higher, speeds decline, and stop-and-go emerges, which indicates a congestion threshold [4–6,8]. Fourth, an Evacuation Parameter Benchmark Library is compiled that covers reaction delay, distributions of speed and acceleration, and cross-area references for density and flow to support parameter inputs and sensitivity analyses in VR and agent-based models.

2 Methodology

Figure 1 summarises the overall workflow, which consists of pre-processing, in-processing, and post-processing.

2.1 Pre-processing

Regarding governance and ethics, video arises from a multi-floor drill under a signed data-sharing memorandum and a low-risk ethics approval. Outputs are de-identified and reported as aggregates and spatial summaries [4–8].

In the scene and BIM frame, lobbies, corridors, and stairwells are covered. The BIM model supplies a common building frame and geometric semantics for camera calibration, area masks, and path topology annotation [4–6].

Thirdly, about camera and time alignment, intrinsics and extrinsics are compiled. When missing, extrinsic parameters are estimated from control points on reference imagery. Streams are synchronised and quality-checked for sharpness and duplication to ensure cross-view comparability.

Furthermore, in the consideration of clip filtering and reduction, motion-present segments are extracted first to reduce empty frames and total duration, which increases signal-to-noise and throughput downstream.

In addition, concerning the issues of spatial calibration and unification plan, planar areas adopt 2D homographs that map pixels into local plane coordinates. Stairwells adopt 3D calibration by sampling control points on landings and sloped flights and by fitting plane equations to support 3D projection and path recovery. Local coordinates are transformed into the building frame via BIM transforms. Robust estimation and reprojection-error thresholds enforce geometric consistency [12].

Lastly, about plenty of parameters, a configuration file fixes detector confidence, NMS, minimum track duration, caps for speed and acceleration, smoothing windows, and the cadence for density estimation. This enables consistent reruns across batches.

2.2 In-processing

To achieve pedestrian detection and multi-object tracking, a modern YOLO detector provides frame-wise person boxes. DeepSORT performs online tracking with appearance embeddings and a Kalman motion model. Dual thresholds on IoU and cosine distance limit identity drift and mismatches [9–11,13,14]. Dense periods use frame decimation and input-size adaptation to balance accuracy and efficiency.

To solve the issue caused by Cross-camera, within a unified timeline, tracklets are stitched across adjacent views using BIM topology constraints and spatiotemporal proximity. Re-association is permitted only within reachable topology and feasible walking windows to curb false merges [4–6].

To process and coordinate the unification need to set. Thus, tracks are first projected to local planes or stair slopes and then mapped to the building frame. RANSAC and reprojection-error thresholds guard geometric consistency and route suspect tracks to review [12].

Continue to trajectory cleaning and physical plausibility, speeds and accelerations are computed by central differences on equal-interval samples and denoised with a 0.5 s moving average [15]. Physical caps remove artefacts, with a speed cap near 4.0 m/s and an acceleration cap near 5.0 m/s. Short occlusions are bridged by multi-hypothesis interpolation with uncertainty recorded. Rules for backtracking, maximum temporal gap, boundary crossing, and abnormal heading change trigger human audits.

The final stage in in-processing, quality logs and versioning are essential. Each batch records detector settings, association rates, retained-track ratios, ID-switch rates, and geometric error distributions. Logs and metadata accompany data packages for comparison and traceability.

2.3 Post-processing analytics

2.3.1 Measures and visualisations

This subsection states the selection principles for measures and visualisations to achieve low bias, portability across scenes, and stable behaviour at high densities while preparing outputs for VR and agent-based calibration.

- Local density uses Voronoi personal space or a fixed-radius kernel. Voronoi yields lower scatter under heterogeneous layouts. Fixed-radius kernels simplify implementation and cross-scene comparison [16].
- Speed and acceleration are computed by central differences with Savitzky–Golay or moving-average smoothing to suppress pixel jitter and tracking noise while retaining temporal resolution [15].
- Uncertainty is expressed with quantile bands and bootstrap confidence intervals to handle skew and heavy tails beyond mean–SD summaries [16,17].
- Bivariate relations use hexbin or equal-frequency bins to limit overplotting. Kernel density estimation is optional when a continuous field is required [16,18].
- Structured indicators include a stair slowdown

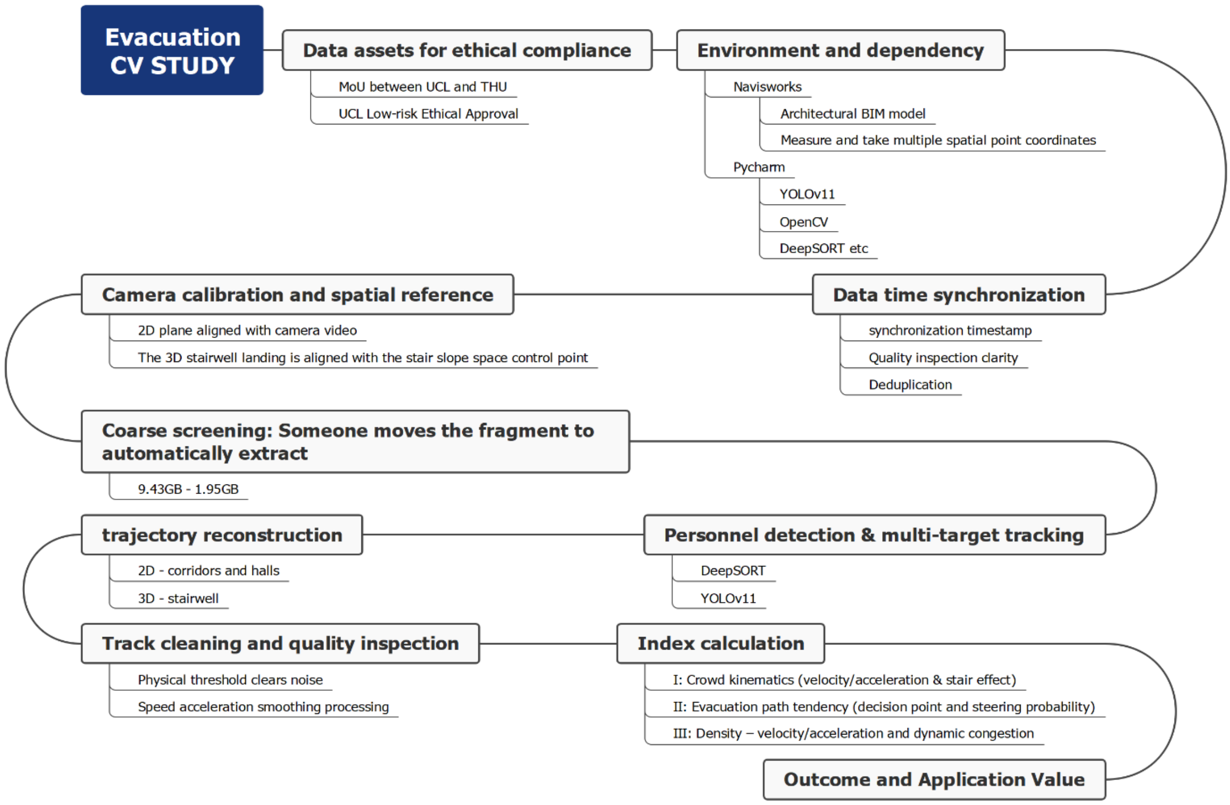

Figure 1 Workflow of Evacuation Computer Vision Tracking Study

factor, an edge-preference index, and a bottleneck score for calibration and sensitivity studies. No thresholds or regime cuts are preset in Methods. They are determined from the data in Results.

2.3.2 Unified formula block

A minimal set of formulas supports three result streams: crowd kinematics (area-wise speed and acceleration), evacuation path tendency (cell-based speed/acceleration heatmaps to reveal decisions and turns), and density–velocity/acceleration with dynamic congestion (1s, 1x1 m2 counts linked to kinematics). Thus, the core formulas are as follows:

$$v_i(t_k) = \frac{[x_i(t_{k+1}) - x_i(t_{k-1})]}{2\Delta t} \quad (1)$$

$$a_i(t_k) = \frac{[v_i(t_{k+1}) - v_i(t_{k-1})]}{2\Delta t} \quad (2)$$

$$\bar{v}_c = mean\{\, ||v_i|| : x_i \text{ in cell } c \,\} \quad (3)$$

$$\bar{a}_c = mean\{\, ||a_i|| : x_i \text{ in cell } c \,\} \quad (4)$$

$$\rho_c(t) = \frac{N_c(t; \Delta t = 1\,s)}{A_c} \quad (5)$$

$$q_c(t) = \rho_c(t) \cdot \bar{v}_c(t) \quad (6)$$

Use (1)–(4): Direct inputs for crowd kinematics by area and for cell-wise speed/acceleration heatmaps (decision/turning zones).

Use (5)–(6): Density axis at one-second cadence and local flow to build density–speed/acceleration relations and identify regimes in Results.

Symbols and parameters:

- x_i, v_i, a_i: position, speed, acceleration vectors
- A_c: cell area (e.g., 0.2 m × 0.2 m)
- $N_c(t;\ \Delta t\ =\ 1\ s)$: unique headcount in cell c within [t, t + 1 s)
- $\bar{v}_c$, $\bar{a}_c$: cell-wise mean speed and acceleration magnitude (quantiles may be used for robustness)
- $\rho_c(t)$: one-second density (persons/m²); $q_c(t)$: local flow

2.3.3 Parameterisation and reproducibility

This subsection summarises parameter settings and reproducibility rules so that outputs remain comparable and traceable across batches in time granularity, smoothing strength, and visualisation strategies.

- One-second density cadence balances frame-level jitter against pedestrian interaction timescales and aligns with common 0.5–1.0 s decision steps in VR or ABM [15,16].
- Smoothing window for kinematics is set near 0.5 s to reduce quantisation noise without lagging peaks materially [15].
- Density-axis cap is fixed at 8 persons per square meter to cover extreme congestion yet avoid unstable extrapolation during fitting [16–18].
- Distributional reporting uses quantile regression and bootstrap to generate trend bands and confidence intervals that remain comparable across floors and areas under skew and heavy tails [16,17].
- Visualisation robustness prefers hexbin or equal-frequency bins to reduce overplotting and sampling bias. KDE is optional for continuous fields, and legends report windows, bandwidths, sample sizes, and exclusion rules for interpretability and reruns [16,17].
- No preset regimes. Thresholds such as free or congested are not specified in Methods. Any segmentation is data-driven and reported in the results after sensitivity checks.

3 Results

This section reports multi-camera trajectory patterns and area-wise kinematics, distils density–movement relations and behavioural tendencies, and delivers reusable benchmarks for calibration.

3.1 Crowd kinematics: area benchmarks

Table 1 compiles representative parameters for calibration and cross-area comparison. Values result from multi-camera trajectory reconstruction with centralised differencing and unified smoothing; density cadence is one second to balance jitter suppression and interaction timescales.

Table 1 Key kinematic parameters by area

Area / Scenario	Mean speed v (m/s)	Mean |a| (m/s²)	Notes
Corridors (2F–4F)	2.072	0.079	Straight corridors permit brief running; 4F start-up means ≈ 1.2; 2F nearer the exit shows higher sustained speeds.
Lobby (ground floor)	1.233	0.071	Merging and route choice broaden the spread; door zones remain slow.
Stair landings	0.524	-0.088	Faster than flights with turning and re-entry at corners.
Stair flights	0.390	0.001	≈25% lower than landings; slowdown factor ≈ 0.75.

3.2 Evacuation path tendency: grid heatmaps

BIM-aligned 0.2 × 0.2 m tiles aggregate speed and acceleration to expose spatial structure. The lobby exhibits a fast perimeter lane and a slow door basin, indicating boundary following and exit coupling. Corridors display a start-up burst to mid-segment dip to pre-door adjustment pattern. Stairwells show speed peaks at landings and acceleration pulses at corners and door thresholds, confirming the landing–flight rhythm. Lobby, stairs and corridor's path trajectory visualisation are shown in Figure 2 to Figure 6.

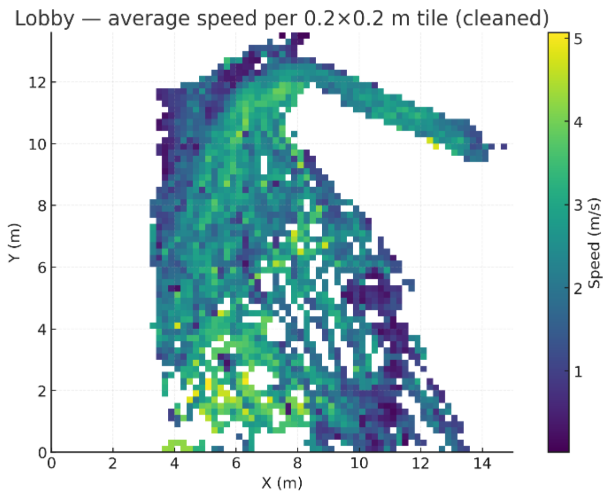

Figure 2 Lobby—average speed per 0.2 × 0.2 m tile (cleaned). Faster edge lane and a slow zone within ~1 m of the exit.

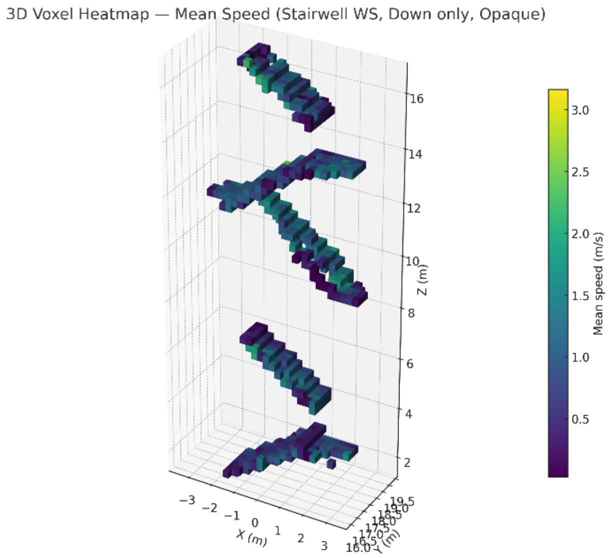

Figure 3 Stairwell WS—3D voxel heatmap of mean speed (down only). Periodic landing–flight texture with faster landings

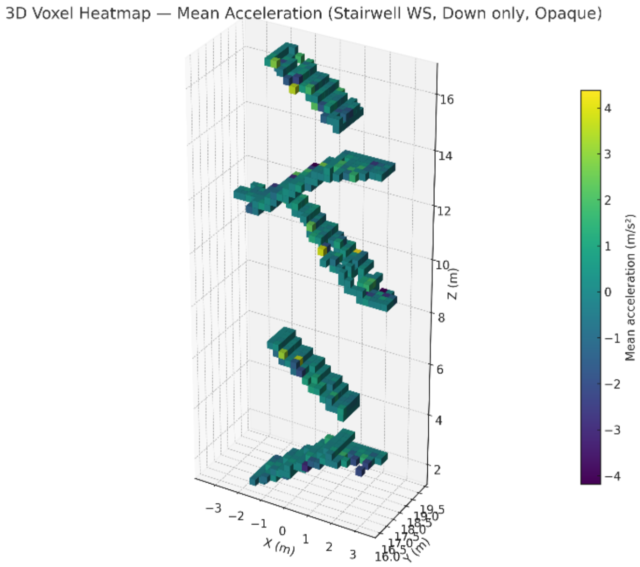

Figure 4 Stairwell WS—3D voxel heatmap of mean acceleration (down only). Pulses at landings and door thresholds indicate braking and restarting.

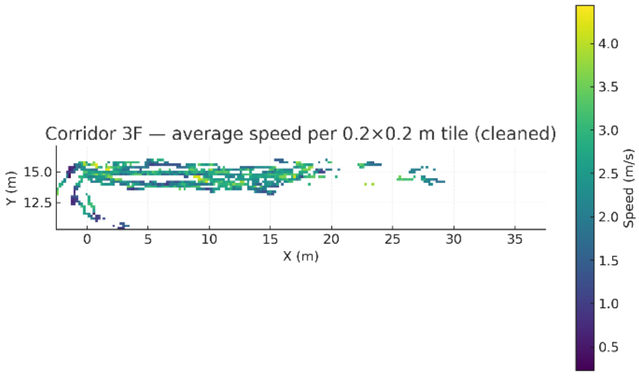

Figure 5 Corridor 3F—average speed per 0.2 × 0.2 m tile. Mid-segment steady; fluctuations near the stair door.

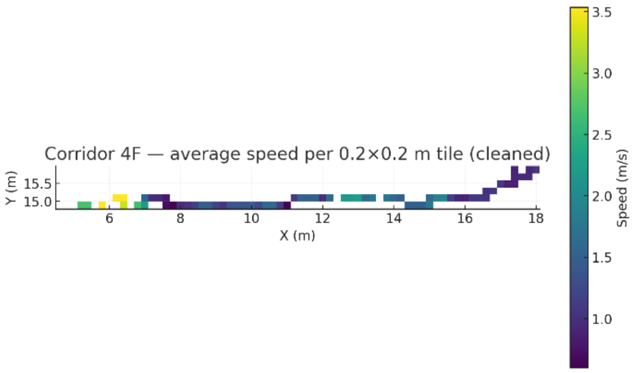

Figure 6 Corridor 4F—average speed per 0.2 × 0.2 m tile. Short start-up acceleration, slowdown near the wall, and accelerate again to the stair area.

3.3 Density–velocity/acceleration and dynamic congestion

Local density ρ is defined as the unique headcount per square meter within one second and is linked to tile-level speed and acceleration. The results are shown in Figure 7 to Figure 8 (Lobby) and Figure 9 to Figure 10 (Stairs).

Lobby. A strong negative density–speed relation is observed: the median speed is ~1–1.5 m/s at ρ≈1–2, falls to ~0.5–0.8 m/s at ρ≈4, and in micro-cells near the exit at ρ≈6–7, speeds are often < 0.5 m/s or momentarily zero. The acceleration–density relation shows maximal variability at moderate density ρ≈2–4, consistent with frequent avoidance and short stop–start movements.

Stairs. The speed–density decline is steeper than on flat areas. Even at ρ≈3–3.5 on landings, speeds converge to ~0.3–0.4 m/s, reflecting tread spacing and safety-distance constraints. Combined with acceleration trends, the evidence indicates that around ρ≈3–4 acceleration dampens markedly while speed changes little, consistent with controlled flow, and that for ρ≥5 speed drops sharply with intermittent movement—consistent with congested flow.

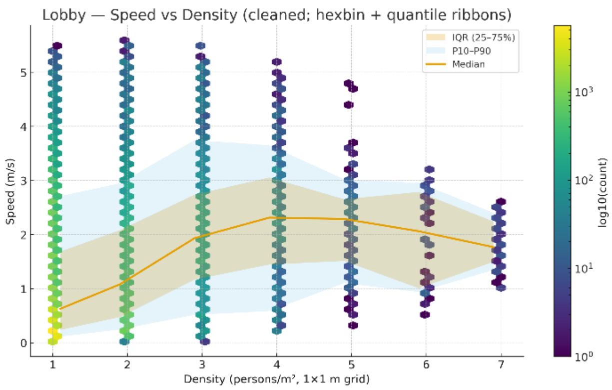

Figure 7 Lobby—Speed vs Density (hexbin with quantile ribbons).

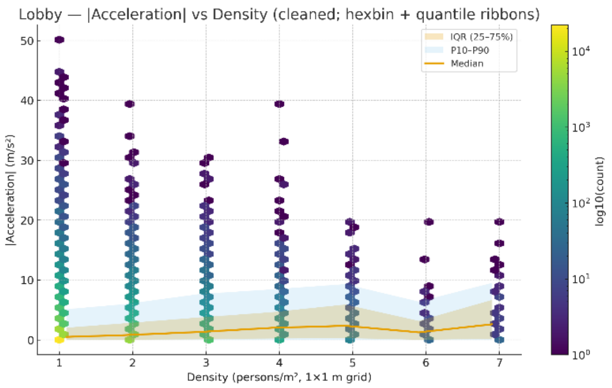

Figure 8 Lobby—|Acceleration| vs Density (hexbin with quantile ribbons).

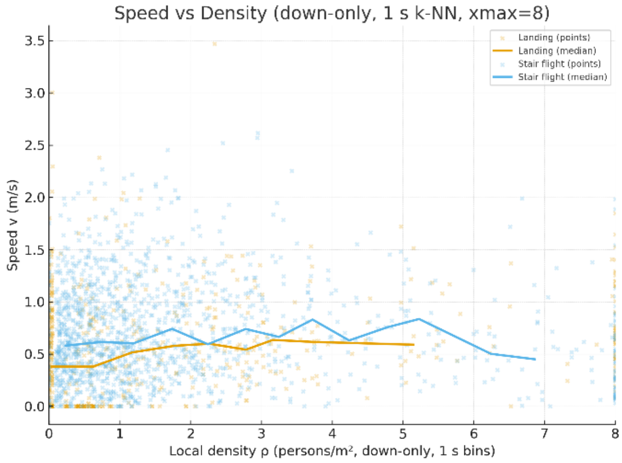

Figure 9 Stairs—Speed vs Density.

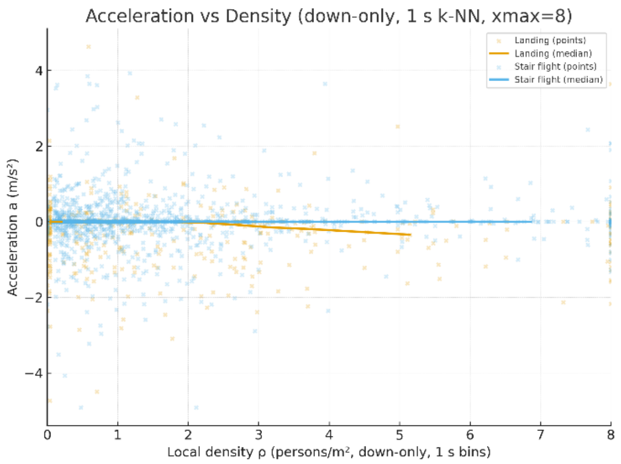

Figure 10 Stairs—Acceleration vs Density.

4 Discussion

The results show pronounced spatial dependence of movement. Corridors support high speeds. The lobby slows under merging and choice. Stairs exhibit a stable landing–flight contrast. Heatmaps (Figures 2–6) reveal fast perimeter lanes, turning nodes, and doorway coupling. Density vs. speed and density vs. acceleration relations (Figures 7 - 10) are consistent with three regimes: free flow (ρ < 3 persons/m²), controlled flow (3 ⩽ ρ ⩽ 5), and congested flow (ρ > 5). Table 1 provides reusable kinematic benchmarks for calibration and design.

4.1 Spatial movement patterns and congestion

Area-specific priors should replace uniform parameters. Table 1 gives representative means for corridors, lobby, and stairs that can anchor prior distributions and validation targets. The stair slowdown factor (~0.75 from landing to flight) parameterises staircase submodels. Speed–density curves should be calibrated by area, with slope and intercept estimated from Figures 7–10. Quantile trends are preferable to mean-only fits to capture heavy tails and heterogeneity. Around $\rho \approx 3–4$, acceleration attenuates while speed changes little. This pattern identifies controlled flow and should be represented by lower stochastic acceleration and higher temporal persistence in velocity updates. Above $\rho \geqslant 5$, speed drops sharply and stop–go emerges, which calls for stronger interaction forces and tighter headway rules.

Path tendency maps (Figures 2–6) provide spatial priors for decision nodes and turn costs. Perimeter bands should carry a lower movement cost to reproduce edge preference, while door cells should carry a higher cost to reproduce slow zones. The landing–flight rhythm in the stair voxel maps supports a periodic turn–align–re-enter sequence with short acceleration pulses that can be encoded as state transitions. Local co-occupancy in corridors must be interpreted with care. Two-person tiles on 2F reflect brief overtakes rather than sustained crowding and should be modelled as transient events, not capacity increases. Route imbalance between twin stairs indicates familiarity and accessibility bias. These biases should be explicit in route choice utilities. Reaction delay should follow a right-skewed distribution with short upper-floor delays and a long lower-floor tail.

4.2 Design and operational implications

Throughput is governed by stair–corridor coupling. Speed troughs and acceleration pulses cluster at landings and door thresholds (Figures 3–4 and 5–6 near stair doors). Priority actions include clearing the first step beyond each door, increasing landing turning radius where feasible, and improving sight lines at corners. The lobby shows a fast perimeter lane and a slow door basin (Figure 2). Centre guidance markings and floor cues can draw flow off walls and reduce corner convergence. Doorway slow zones warrant checks of clear width, door swing, and obstacle placement. Twin-stair imbalance highlights that adding exits does not guarantee balanced use. Training and dynamic signage can redistribute demand in real time. High corridor speeds raise fall and collision risk during emergencies. Non-slip finishes, local slowdown cues, and staff positioning at corners and exits can mitigate these risks.

4.3 Limitations and future work

The drill involved about ninety participants and reflects moderate loading. Extreme congestion appears in micro-cells near the exit. Extrapolation to extremely high densities should be cautious. Occlusion and camera geometry can cause occasional track loss. Spatial quantisation and smoothing may damp noticeably short peaks in speed or acceleration. Geometry is site-specific, including stair width, tread rise–run, and doorway layout, so cross-building transfer requires recalibration. The benchmark represents the first step toward a VR evacuation parameter library. Expansion is needed across occupancies and layouts, broader building typologies, and outdoor domains such as forecourts and sidewalks. Higher-density drills should bound performance in congested regimes. Standardised schemas, quality control, and uncertainty reporting will support reuse. With progressive release of parameters and visual assets, calibrated immersive studies can feed validated insights back into performance-based egress design and operations.

5 Conclusion

An automated multi-camera pipeline aligned to BIM reconstructed 2D/3D evacuation trajectories across corridors, lobby, and stairs. Results deliver a reusable, multi-area benchmark for VR and agent-based calibration. Corridors supported higher speeds (overall mean $\approx$ 2.07 m/s). The lobby averaged $\approx$ 1.23 m/s under merging and choice. Stairs showed a stable geometric effect with means $\approx$ 0.52 m/s on landings and $\approx$ 0.39 m/s on flights, implying a slowdown factor $\approx$ 0.75. Density and speed were negatively related beyond $\approx$ 2 persons/m^2. Acceleration variability peaked at moderate density. Edge preference and doorway slowdowns dominated open areas. Twin stairs showed route imbalance. Reaction times were right-skewed with short upper-floor delays and a lower-floor long tail.

These outputs constitute the first step toward a VR evacuation parameter benchmark library. Area-specific speed and acceleration distributions provide priors and validation targets. The stair slowdown factor parameterises staircase submodels. Density–speed and density–acceleration curves set quantitative goals for interaction strength and stochastic noise. Edge preference and door penalties can be encoded in path-cost fields to reproduce observed streamlines. The intended outcome is a practical feedback loop where calibrated immersive studies inform real-world egress planning and operations.

Current limits include moderate loading, site-specific geometry, and potential occlusions. Next steps expand coverage across different occupancies and layouts, additional interior zones such as atria and large assembly spaces, and outdoor domains including forecourts and sidewalks. Higher-density drills will bound congested-regime performance. Standardised schemas, quality control, and uncertainty reporting will support reuse. Progressive public release of parameters and visual assets will grow the library into a shared reference for performance-based design and for immersive technologies that return validated insights to practice. Accordingly, the contribution lies not in universal parameter claims, but in a reproducible workflow for deriving space-specific benchmarks from real drills.

Acknowledgement

This work was supported by the Horizon Europe Project, D-HYDROFLEX (Grant Number 101122357), the Horizon Europe Project, INHERIT (Grant Number 101123326), and the ISPF British Council funded EyeISENS project. This research was supported in part by the National Key R&D Program of China (2024YFE0114400) and supported by UCL BSSC Conference Funding.

Reference

[1] Cimellaro GP, Domaneschi M, de Iuliis M, Villa V, Caldera C, Cardoni A. Fire emergency evacuation in a school building through VR. vol. 1, 2019, p. 2046–55.

[2] Yu D, Mahamadu Abdul-Majeed, Chen, Weiwei. Integration of Immersive Technology and Digital Twins for Emergency Management in Buildings: A Systematic Literature Review 2024. https://doi.org/10.13140/RG.2.2.11050.84160.

[3] Yu D, Chen W, Meng T, Yu H, Mahamadu A-M. Applications of Immersive Technologies in Construction Computing: A Systematic Literature Review. Computing in Construction 2024;5.

[4] Ding Y, Chen X, Zhang Y, Huang X. Smart building evacuation by tracking multi-camera network and explainable Re-identification model. Engineering Applications of Artificial Intelligence 2025;148:110394. https://doi.org/10.1016/j.engappai.2025.110394.

[5] Zhang X, Chen X, Ding Y, Zhang Y, Wang Z, Shi J, et al. Smart real-time evaluation of tunnel fire risk and evacuation safety via computer vision. Saf Sci 2024;177. https://doi.org/10.1016/j.ssci.2024.106563.

[6] Li S, Tong L, Zhai C. Extraction and modelling application of evacuation movement characteristic parameters in real earthquake evacuation video based on deep learning. Int J Disaster Risk Reduct 2022;80. https://doi.org/10.1016/j.ijdrr.2022.103213.

[7] Ding Y, Chen X, Wang Z, Zhang Y, Huang X. Human behaviour detection dataset (HBDset) using computer vision for evacuation safety and emergency management. Journal of Safety Science and Resilience 2024;5:355–64. https://doi.org/10.1016/j.jnlssr.2024.04.002.

[8] Huang S, Ji J, Wang Y, Li W, Zheng Y. A machine vision-based method for crowd density estimation and evacuation simulation. Safety Science 2023;167:106285. https://doi.org/10.1016/j.ssci.2023.106285.

[9] Xue Z, Kong L, Wu H, Chen J. Fire and Smoke Detection Based on Improved YOLOV11. IEEE Access 2025;13:73022–40. https://doi.org/10.1109/ACCESS.2025.3564434.

[10] Jiang Y, Liu P, Han Y, Xiao B. YOLOv11-CHBG: A Lightweight Fire Detection Model. Fire 2025;8:338. https://doi.org/10.3390/fire8090338.

[11] Reddy VSR, Chintala KS, M Amsaprabhaa, S Vidhusha. A Vision-based Gait Analysis and Fall Detection Using YOLOv11 Model. 2025 International Conference on Wireless Communications Signal Processing and Networking (WiSPNET), Chennai, India: IEEE; 2025, p. 1–7. https://doi.org/10.1109/WiSPNET64060.2025.11004995.

[12] Fischler MA, Bolles RC. Random sample consensus: a paradigm for model fitting with applications to image analysis and automated cartography. Commun ACM 1981;24:381–95. https://doi.org/10.1145/358669.358692.

[13] Wojke N, Bewley A, Paulus D. Simple online and realtime tracking with a deep association metric. 2017 IEEE international conference on image processing (ICIP), IEEE; 2017, p. 3645–9.

[14] Kalman RE. A new approach to linear filtering and prediction problems 1960.

[15] Savitzky Abraham, Golay MJE. Smoothing and Differentiation of Data by Simplified Least Squares Procedures. Anal Chem 1964;36:1627–39. https://doi.org/10.1021/ac60214a047.

[16] Silverman BW. Density estimation for statistics and data analysis. Routledge; 2018.

[17] Koenker R, Bassett G. Regression Quantiles. Econometrica 1978;46:33. https://doi.org/10.2307/1913643.

[18] Lewin-Koh N. Hexagon binning: an overview 2024.